IEEE Open Journal of
Power Electronics

Received 24 March 2020; revised 9 May 2020; accepted 10 May 2020. Date of publication 21 May 2020; date of current version 4 June 2020. The review of this article was arranged by Associate Editor Zhixiang Zou.

Digital Object Identifier 10.1109/OJPEL.2020.2996427

Single-Phase Grid-Connected Inverters With Simplified SPWM Control

NOOR SYAFAWATI AHMAD (Member, IEEE), TERNG-WEI TSAI (Student Member, IEEE), AND YAOW-MING CHEN (Senior Member, IEEE)

Electric Energy Processing Laboratory (EEPro), Department of Electrical Engineering, National Taiwan University, Taipei 10617, Taiwan

CORRESPONDING AUTHOR: YAOW-MING CHEN (e-mail: ntuymchen@ieee.org)

ABSTRACT The conventional grid-connected inverters require a sophisticated digital signal processor to generate the demanded reference signal as a feedforward signal for the sinusoidal pulse width modulation (SPWM) control. However, the reference signal needs to be re-calculated to maintain the demanded power control as the ac mains varies. It increases the computation burden of the controller and has become a major obstacle of the grid connected energy storage system with demanded power flow control. Therefore, a simplified approach to reduce the computation burden of the controller is proposed in this paper. With the proposed simplified equation for the power flow control, the usage of a low cost microcontroller unit becomes possible. In additional, no additional sensors or circuitries are needed. Meanwhile, the performance of desired power flow control by using the simplified control is almost unaffected. The proposed simplified algorithm is validated via mathematical calculations, computer simulation and experimental results. By using the proposed simplified control, 52.3% of the computational clock cycles can be reduced. Different operation scenarios were tested to validate the performance of the proposed simplified control via the MATLAB/Simulink simulations and the 1kVA prototype experiments.

INDEX TERMS Grid-Connected Inverters, Pulse Width Modulation, Power Flow Control, Digital Signal Processing.

I. INTRODUCTION

The renewable energy source has drawn a lot of attention due to the energy shortage and environment issues. Moreover, the energy consumption increases the demand for renewable energy such as wind and solar. The renewable energy resources as distributed generations (DGs) have become more important and caused the research on microgrid intensely. The microgrid is attractive because the conventional electric power system is stressed by the limitation of power delivery capability, the exponential growth of power demand, and complication in building new transmission and distribution lines [1]–[4].

A microgrid is an active distribution network that can be utilized in either the islanding mode or the grid-connected one. In the microgrid, the DGs are always connected to power network through power inverters. In islanding mode, the inverter works as a voltage controlled source, where the microgrid has to control the power balance independently as it disconnects from the main grid [5], [6]. Also, the intention of the islanding mode is to increase the reliability of the power supply in rural feeders and to sustain human development [7]. In the grid-connected mode, different DGs are connected in parallel to the microgrid via the current controlled inverters to supply local loads and possibly feed power into the main grid. Those grid-connected DGs need to meet the grid codes or national standards such as power factor and total harmonic distortion [5], [8]–[10].

Therefore, grid-connected inverters have to achieve five basic features: 1) the active power delivered to the grid; 2) the reactive power transfer between the grid and the distributed power generation system; 3) the DC-link voltage balance; 4) assuring high quality of the injected power; and 5) grid synchronization. Also, the grid operator may request auxiliary services such as voltage harmonic compensation, active filtering, or local frequency and voltage regulation [11].

On the other hand, in dealing with the inherent intermittent nature of the renewable energy source, the energy storage

device, such as a battery bank, plays an important role and is commonly adopted to accommodate the variation of the available power generation and demand [12]–[14]. The energy storage device alone with the grid-connected inverter can supply uninterruptable power flow to the microgrid to improve the power system's stability and reliability [15], [16]. As a results, the grid-connected voltage source inverter (GVSI) becomes an important key component in modern power system [17]–[20].

Many circuit topologies have been proposed to implement the GVSI. Among them, the full-bridge topology is the most commonly seen and can be applied to different applications, including the uninterrupted power supply [21], [22]. For the GVSI, due to the ac mains voltage, the sinusoidal pulse-width modulation (SPWM) becomes the most commonly used control method [23]. The advantages of SPWM include the realization of frequency modulation and voltage regulation at the same time, rapid dynamic response, and low frequency harmonics elimination. Therefore, the SPWM has been adopted in many GVSIs [24]–[26].

The control function of a GVSI can be divided into two major tasks: power and current control. Usually, the outer control loop is used to control the real and reactive power flow between the DGs and the microgrid. The inner control loop is mainly for the current control to mitigate the high frequency disturbances and damp the output LC filter to avoid resonance with the external network [13]. However, these control strategies have to interact with many system parameters and it requires a high end and high cost digital signal processor (DSP).

The control schemes focus on the controllability of the GVSI operated within the microgrid are discussed and analyzed [18], [19]. The improvement, not limited in circuit topology and yet the algorithm to decrease the switching loss or to cancel out the oscillations caused by the harmonic voltage distortion have been proposed [27], [28]. A review to classify the existing control schemes for the GVSI to act as a power quality conditioner has been discussed [29].

Meanwhile, a modularized bidirectional single-phase grid-connected inverter with a control strategy which allows it to operate in inverter mode or rectified mode has been proposed [30]. Because of these operation modes, it needs to inject/draw a sinusoidal current into/from the ac mains. However, the control strategy is a hysteresis-based control scheme, which has fast dynamic response and simple circuit yet it has to deal with variable switching frequency operation that burden the controller in completing the switching frequency calculation. Therefore, it is the motivation to develop a simpler equation, which can reduce the computational burden by using the SPWM control method, and is able to sustain the grid voltage fluctuations,

In this paper, a simplified algorithm using SPWM control strategy is proposed for the GVSI that can be operated under grid voltage fluctuation while maintaining the constant demanded active and reactive power delivery. For the SPWM control strategy, a sinusoidal waveform as the reference signal is generated to do the comparison with the triangular

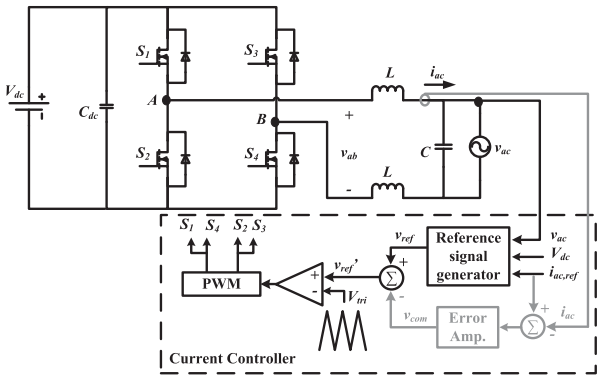

FIGURE 1. Schematic diagram of GVSI with current control.

waveform to generate the pulsating gate signal. The reference signal consists of the parameters such as the ac mains voltage and the output current amplitude. Therefore, the conventional approach to obtain the reference signal requires many computational works to accomplish the mathematical solving. The computational burden should be reduced to increase the switching speed, the system's dynamic response, and to utilize a lower level microcontroller unit in order to reduce the cost. Also, with the reduced computation time, the controller can save time resource to accomplish more tasks such as THD monitoring or multiple power module control.

Therefore, this paper focuses on the develop of a simplified reference signal generation in order to reduce the computational burden. The mathematical derivation of the reference signal is introduced in Section II, followed by the proposed simplified equation, which is derived in Section III. In addition, the validation of the proposed simplified equation is presented in Section IV. Finally, the computer simulations and experimental investigations of the proposed simplified control algorithm is verified by a laboratory prototype in Section V.

II. MATHEMATICAL DERIVATION

A single-phase full-bridge GVSI with a SPWM current controller is depicted in Fig. 1. The full-bridge GVSI is composed of four power switches, an LC filter and a current controller. The current controller consists of a reference signal generator, current error amplifier, and a comparator with PWM switching signals.

As shown in Fig. 1, three parameters, ac mains voltage v_{ac}, dc voltage V_{dc} and reference ac current $i_{ac,ref}$, are required to generate the feedforward sinusoidal control signal v_{ref} for the PWM gate signal comparator. On the other hand, to compensate the output current distortion, the output current is sensed and compared with the reference current alone with an error amplifier to form a feedback current control. The compensated sinusoidal reference signal, $v_{ref}{}'$ and the triangular carrier, V_{tri} waveform are compared to generate the PWM gate signals for the power switches. Since the objective of the proposed simplified control method is to transfer the demanded constant power under the fluctuated ac mains voltage, the reference signal generator in the feedforward loop is focused.

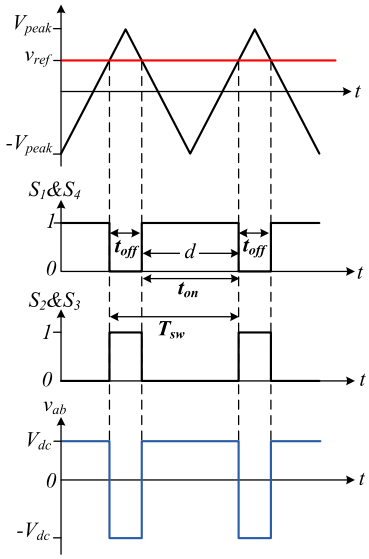

FIGURE 2. Typical key waveforms of gate signal generation using SPWM method.

The key waveforms of typical SPWM strategy for two switching cycles are shown in Fig. 2. The sinusoidal reference signal v_{ref} can be illustrated as the red straight line because the switching frequency is much higher than line frequency. The duty ratio d of the gate signal determines the complementary turn-on time, t_{on}, and turn-off time, t_{off}, for the switches pair, $S_1\&S_4$ and $S_2\&S_3$, respectively.

The voltage v_{ab} across the terminals A and B in Fig. 1 is either $+V_{dc}$ or $-V_{dc}$. By modulating d, the voltage v_{ab} can be controlled. By referring to the waveforms shown in Fig. 2, the duty ratio d of the inverter can be written as:

$$d = \frac{1}{2} + \frac{v_{ref}}{2V_{peak}} \tag{1}$$

where V_{peak} is the peak value of the triangular waveform, V_{tri}.

The equivalent value of v_{ab} within one switching period is expressed as:

$$v_{ab} = [V_{dc} \times d] + [-V_{dc} \times (1-d)] = [2d-1]\,V_{dc} \tag{2}$$

By substituting (1) into (2), the expression of the voltage at terminal A and B becomes:

$$v_{ab} = \left(\frac{V_{dc}}{V_{peak}}\right) v_{ref} \tag{3}$$

From Fig. 1, the relation of v_{ab}, v_{ac} and i_{ac} across the inductor L in steady-state can be derived as:

$$v_{ab} - v_{ac} = L\frac{di_{ac}}{dt} \tag{4}$$

Substituting (3) into (4) results in the following equation of the steady-state current expression in phasor form:

$$\vec{i}_{ac} = \frac{\left(\frac{V_{dc}}{V_{peak}}\right)\vec{v}_{ref} - \vec{v}_{ac}}{j\omega L} \tag{5}$$

where ω is the angular frequency of the ac mains and the right arrow on the top of i_{ac}, v_{ref} and v_{ac} represents the phasor form. As shown in (5), the current control of i_{ac} requires the determination of the reference signal and the grid voltage.

The current control block shown in Fig. 1 is used to fulfill the SPWM gate signal generation, where the sinusoidal reference signal generator is included in the feedforward path and the current compensation is accomplished by the error amplifier in the feedback path in grey color. To generate the sinusoidal reference signal, v_{ref}, for the SPWM control, it requires the information of dc voltage, ac mains voltage, and line current. The goal of the control strategy is to make the ac mains current i_{ac} equal to the desired reference current $i_{ac,ref}$. To do so, an appropriate sinusoidal reference signal needs to be generated. Thus, (5) is rearranged into (6) to determine the $\vec{v}_{ref}$.

$$\vec{v}_{ref} = \frac{V_{peak}}{V_{dc}}\left[\vec{v}_{ac} + j\omega L\,\vec{i}_{ac,ref}\right] \tag{6}$$

To facilitate the phasor form of reference signal calculation in (6), the magnitude, $|\vec{v}_{ref}|$ and the phase angle, $\angle\theta_{ref}$ of the $\vec{v}_{ref}$ can be derived as below:

$$\left|\vec{v}_{ref}\right| = \frac{V_{peak}}{V_{dc}}\sqrt{\begin{array}{l}\left|\vec{v}_{ac}\right|^2 + \omega^2L^2\left|\vec{i}_{ac,ref}\right|^2 \\ -2\omega L\left|\vec{v}_{ac}\right|\left|\vec{i}_{ac,ref}\right|\sin(\theta_i - \theta_v)\end{array}} \tag{7}$$

$$\angle\theta_{ref} = \tan^{-1}\left[\frac{\left|\vec{v}_{ac}\right|\sin\theta_v + \omega L\left|\vec{i}_{ac,ref}\right|\cos\theta_i}{\left|\vec{v}_{ac}\right|\cos\theta_v - \omega L\left|\vec{i}_{ac,ref}\right|\sin\theta_i}\right] \tag{8}$$

where $|\vec{v}_{ac}|$, $|\vec{i}_{ac}|$ is the amplitude of v_{ac} and i_{ac}, θ_i is the phase angle of the ac mains current, θ_v is the phase angle of the ac mains voltage which can be assumed to be 0°.

When the ac mains voltage is fluctuated from the nominal value, the reference signal needs to be renewed. From (7) and (8), the updated reference signal equation can be expressed as below:

$$\left|\vec{v}_{ref,new}\right| = \frac{V_{peak}}{V_{dc}}\sqrt{\begin{array}{l}\left|\vec{v}_{ac.new}\right|^2 + \omega^2L^2\left|\vec{i}_{ac.new}\right|^2 \\ -2\omega L\left|\vec{v}_{ac.new}\right|\left|\vec{i}_{ac.new}\right|\sin(\theta_i)\end{array}} \tag{9}$$

$$\angle\theta_{ref,new} = \tan^{-1}\left[\frac{\omega L\left|\vec{i}_{ac.new}\right|\cos\theta_i}{\left|\vec{v}_{ac.new}\right| - \omega L\left|\vec{i}_{ac.new}\right|\sin\theta_i}\right] \tag{10}$$

where $|\vec{v}_{ref,new}|$ and $\angle\theta_{ref,new}$ are the new values of magnitude and phase angle of the $\vec{v}_{ref}$, while $|\vec{v}_{ac,new}|$ and $|\vec{i}_{ac,new}|$ are the amplitude of the new ac mains voltage and current, respectively.

The block diagram representations of (9) and (10) are illustrated in Fig. 3(a) and (b), respectively. As clearly depicted in Fig. 3, both magnitude and phase angle of the reference

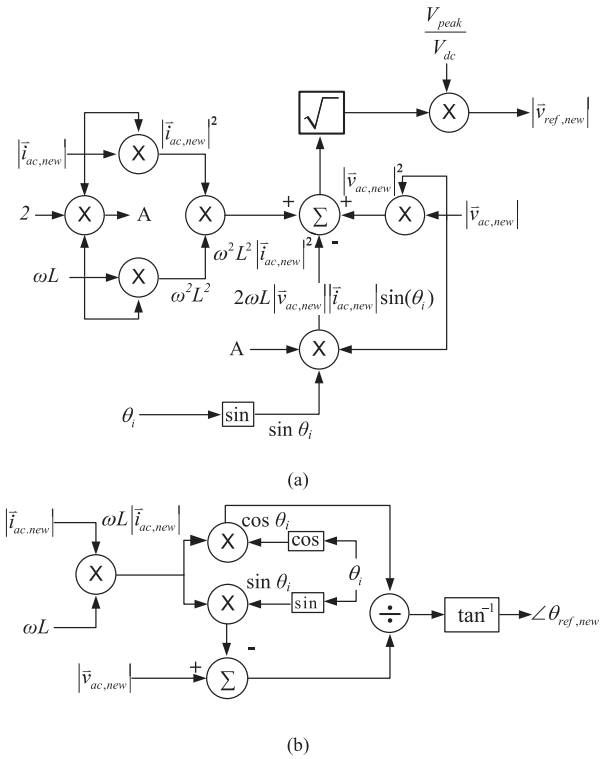

FIGURE 3. The computation block diagrams of conventional reference signal under fluctuated ac mains voltage $\vec{v}_{ac,new}$. (a) The magnitude of the reference signal $|\vec{v}_{ref,new}|$ in (9). (b) The phase angle of the reference signal $\angle\theta_{ref,new}$ in (10).

signal need to be re-calculated if the ac mains voltage fluctuates. However, the calculation requires numerous mathematical operations which increases the computational burden of the controller.

III. PROPOSED SIMPLIFIED EQUATION

In this paper, the inverter is designed to operate under fixed demanded apparent power. Under the demanded power condition, the magnitude $|\vec{i}_{ac,ref}|$ and phase angle θ_i of the ac mains current can be expressed as below:

$$\left|\vec{i}_{ac,ref}\right| = \frac{\sqrt{P^2+Q^2}}{\left|\vec{v}_{ac}\right|} \tag{11}$$

$$\theta_i = -\tan^{-1}\frac{Q}{P} \tag{12}$$

where P is the active power and Q is the reactive power. By combining (9) through (12), the mathematical expression of the new reference signal can be derived as following equations:

$$\left|\vec{v}_{ref,new}\right| = \frac{V_{peak}}{V_{dc}}\sqrt{\left|\vec{v}_{ac,new}\right|^2 + \frac{\omega^2L^2\left(P^2+Q^2\right)}{\left|\vec{v}_{ac,new}\right|^2} + 2\omega LQ} \tag{13}$$

$$\angle\theta_{ref,new} = \tan^{-1}\left[\frac{\omega LP}{\left|\vec{v}_{ac,new}\right|^2 + \omega LQ}\right]. \tag{14}$$

Referring to (13) and (14), the phase angle in (14) becomes simpler compared to (10), but not for the magnitude as in (13). Hence, the simplification derivation is focused on the magnitude of the reference signal. Because the objective of the GVSI is to maintain the consistent power control under the variable line voltage condition, the amplitude of the new ac mains voltage and current can be expressed by the summation of the nominal value and the variation as shown below:

$$\left|\vec{v}_{ac,new}\right| = V_{ac} + \Delta v_{ac} \tag{15}$$

$$\left|\vec{i}_{ac,new}\right| = I_{ac} + \Delta i_{ac} \tag{16}$$

where $|\vec{v}_{ac,new}|$ and $|\vec{i}_{ac,new}|$ is the amplitude of the new ac mains voltage and current, respectively. Also, V_{ac} and I_{ac} are the nominal value of the ac mains voltage and current. Meanwhile, Δv_{ac} and Δi_{ac} are the variation values of the $|\vec{v}_{ac,new}|$ and $|\vec{i}_{ac,new}|$ over the nominal voltage and current.

Since the $|\vec{v}_{ac,new}|$ is the main trigger for the calculation process, a variation index, k is developed for the proposed simplified method. The variation index k is defined as the variation ratio of the voltage and can be expressed as:

$$k = \frac{\left|\vec{v}_{ac,new}\right| - V_{ac}}{V_{ac}} = \frac{\Delta v_{ac}}{V_{ac}}. \tag{17}$$

It should be noted that the detection of the ac mains voltage in every cycle is an existing required feature in the GVSI. Hence, no additional circuitry is required for the proposed method. Since the GVSI is expected to deliver the same demanded S under varying ac mains voltage, the nominal S is equal to new S as expressed below:

$$V_{ac}I_{ac} = \left|\vec{v}_{ac,new}\right|\left|\vec{i}_{ac,new}\right|. \tag{18}$$

By substituting (15), (16), and (17) into (18), the following expression is obtained:

$$\Delta i_{ac} = -\frac{\Delta v_{ac}}{V_{ac}}I_{ac} = -kI_{ac} \tag{19}$$

where the term $\Delta v_{ac}\Delta i_{ac}$ is relatively small and can be neglected.

Hence, (15) and (16) can be substituted into (9) which yields:

$$\left|\vec{v}_{ref,new}\right| = \frac{V_{peak}}{V_{dc}}\sqrt{\begin{array}{c}(V_{ac}+\Delta v_{ac})^2 + \omega^2L^2(I_{ac}+\Delta i_{ac})^2 \\ -2\omega L\,(V_{ac}+\Delta v_{ac})\,(I_{ac}+\Delta i_{ac})\sin\theta_i\end{array}}. \tag{20}$$

By solving and rearranging (20) with the assumption that Δv_{ac}^2, Δi_{ac}^2, $\Delta v_{ac}\Delta i_{ac}$ are relatively small and are neglected,

then (21) can then be obtained:

$$\left|\vec{v}_{ref,new}\right| \approx \frac{V_{peak}}{V_{dc}} \sqrt{\begin{matrix} {V_{ac}}^2 + \omega^2 L^2 {I_{ac}}^2 - 2\omega L V_{ac} I_{ac} \sin\theta_i \\ + \left[\begin{matrix} 2V_{ac}\Delta v_{ac} + 2\omega^2 L^2 I_{ac}\Delta i_{ac} \\ -2\omega L\left(V_{ac}\Delta i_{ac} + I_{ac}\Delta v_{ac}\right)\sin\theta_i \end{matrix}\right] \end{matrix}}. \quad (21)$$

It is understandable that both (7) and (21) are related since they are the equations for the magnitude of the v_{ref}. In other words, the new magnitude of the v_{ref} can be written as:

$$\left|\vec{v}_{ref,new}\right| = \left|\vec{v}_{ref}\right| + \Delta v_{ref} \quad (22)$$

where $|\vec{v}_{ref}|$ is the magnitude defined from (7) using nominal value and Δv_{ref} is the variation of the $|\vec{v}_{ref,new}|$. Equation (22) reveals that only the Δv_{ref} is required to be re-calculated in order to update the value of $|\vec{v}_{ref,new}|$. From (7), (21), and (22), the following equation can be obtained:

$$\Delta v_{ref} = \left(\frac{V_{peak}}{V_{dc}}\right)^2 \left(\frac{V_{ac}\Delta v_{ac} + \omega^2 L^2 I_{ac}\Delta i_{ac} - \omega L\left(V_{ac}\Delta i_{ac} + I_{ac}\Delta v_{ac}\right)\sin\theta_i}{\left|\vec{v}_{ref}\right|}\right). \quad (23)$$

The expression of Δv_{ref} can be simplified by substituting (11), (12), (17), and (19) into (23). Eventually, a concise expression of Δv_{ref} can be written as:

$$\Delta v_{ref} = \left(\frac{V_{peak}}{V_{dc}}\right)^2 \left(\frac{{V_{ac}}^4 - \omega^2 L^2\left(P^2+Q^2\right)}{{V_{ac}}^2\left|\vec{v}_{ref}\right|}\right) \cdot (k) \quad (24)$$

where $(\frac{V_{peak}}{V_{dc}})^2(\frac{{V_{ac}}^4-\omega^2L^2(P^2+Q^2)}{{V_{ac}}^2|\vec{v}_{ref}|})$ consists of constant nominal values, and is denoted as N. Hence, the new magnitude of v_{ref} in (22) can be rewritten as:

$$\left|\vec{v}_{ref,new}\right| = \left|\vec{v}_{ref}\right| + N \cdot k. \quad (25)$$

Eventually, the mathematical block diagrams to compute the magnitude (25) and phase angle (14) of the new reference signal are shown in Fig. 4. By comparing to the block diagram shown in Fig. 3, the computation in Fig. 4 appears to be much simpler. To further confirm the computational burden reduction, the instruction clock cycles required by MCU/DSP to execute the mathematical operations in (9), (10), (14) and (25), or in Fig. 3 and Fig. 4, are analyzed. Fig. 5 shows the required number of clock cycles, which is obtained based on the instruction set specification of Texas Instruments TMS320C28x MCU/DSP controller [31]. Fig. 5 shows a bar chart to present the required clock cycles comparison. As evidently shown in Fig. 5, the proposed simplified equations (14) and (25), in red color bar, require significantly less clock cycles than that required by conventional equations (9) and (10) in blue color bar. The overall reduction in computational burden achieved by the proposed simplified equations is, more than 52% as shown in Fig. 5.

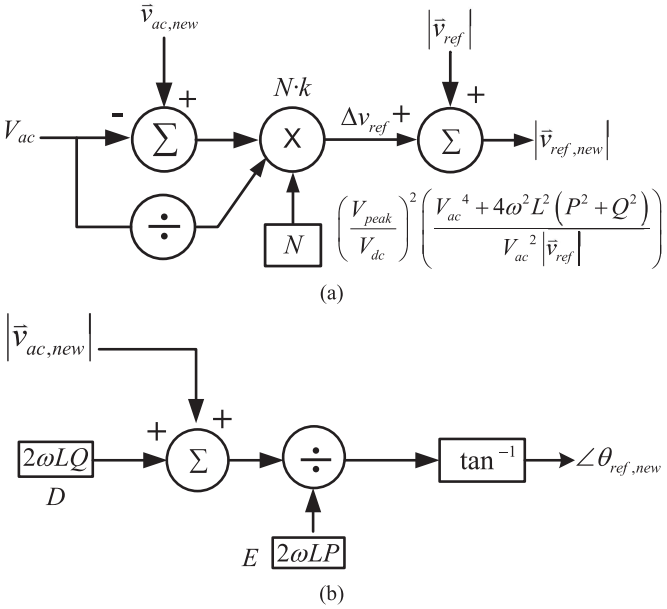

FIGURE 4. Block diagram of proposed simplified equation of the reference signal under new ac mains voltage $v_{ac,new}$. (a) The magnitude of the reference signal $|\vec{v}_{ref,new}|$ in (25). (b) The phase angle of the reference signal $\angle\theta_{ref,new}$ in (14).

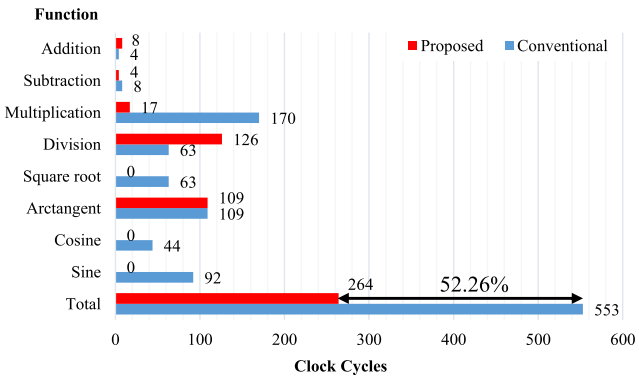

FIGURE 5. The comparison of the clock cycle counts for the conventional and the proposed simplified equations of the reference signal.

The proposed simplified control algorithm can also achieve similar computing time reduction for high-level DSPs with hardware acceleration units and various programming languages.

IV. MATHEMATICAL VALIDATION

Although the proven proposed simplified equation had reduced the computational burden, the accuracy of using the proposed approach will be verified in this section. The specifications of the inverter shown in Table 1 is used to show the accuracy of the proposed equation via mathematical validation, computer simulation and prototype experiment.

TABLE 1. Specification of the Single-Phase Full-Bridge Inverter

Parameter	Symbol	Value
demanded apparent power	S	1 kVA
ac mains voltage	V_{ac}	110 V_{rms}
dc voltage	V_{dc}	200 V
output inductor	L	2 mH
output capacitor	C	0.1 μF
line frequency	f	60 Hz
switching frequency	f_{sw}	30 kHz

TABLE 2. Magnitudes and Errors of the Reference Signals for Under Different Δv_{ac} and Power Rating

Power rating	P = 600W; Q = 800VAR			P = 800W; Q = 600VAR			P = 1000W; Q = 0VAR		
Δv_{ac} (%)	(9)	(25)	Error (%)	(9)	(25)	Error (%)	(9)	(25)	Error (%)
-20	102.27	101.60	0.62	99.23	98.67	0.57	89.65	89.36	0.33
-15	106.84	106.51	0.31	103.98	103.68	0.29	94.88	94.73	0.16
-10	111.56	111.42	0.12	108.82	108.70	0.11	100.16	100.10	0.16
-5	116.37	116.33	0.03	113.75	113.72	0.03	105.49	105.48	0.01
0	121.25	121.25	0.00	118.73	118.73	0.00	110.85	110.85	0.00
5	126.19	126.16	0.02	123.78	123.75	0.02	116.24	116.60	0.04
10	131.18	131.07	0.09	128.86	128.77	0.08	121.06	121.97	0.07
15	136.22	135.98	0.18	133.99	133.78	0.16	127.06	126.97	0.07
20	141.13	140.90	0.29	139.15	138.80	0.26	132.49	132.34	0.11

The new magnitude of the reference signal for the conventional and the simplified equations derived in (9) and (25) are calculated and compared in this section. For the validation, both equations for the $|\vec{v}_{ref.new}|$ are calculated under different ac mains voltage. Table 2 shows the tabulation of the calculations of the new magnitude of the reference signal using (9) and (25), where Δv_{ac} are set between the range of +20% to −20%. The error percentage on Table 2 is defined as the ratio of the magnitude value difference between (25) and (9) over the value of (9).

From the calculated results shown in Table 2, the proposed simplified equation (25) can obtain relatively small difference by referring to (9). It shows that the error percentage of (25) remains below 0.62% even though the ac mains has reached a 20% fluctuation, which is much larger than the commonly used grid code.

Through the mathematical validation shown in Table 2, the performance of the proposed simplified equation using (25) can be organized into different set of conditions to verify the accuracy of the reference signal through computer simulations and experimental measurements. In order to validate the proposed method, the system is divided into three different profiles as discussed in the following sections.

TABLE 3 The Classification of Profiles under Variation of Δv_{ac} (%)

Profile	Δv_{ac} (%)	Peak ac voltage (V)
Normal	0	155.56
Case I	-15	132.23
Case II	+15	177.63

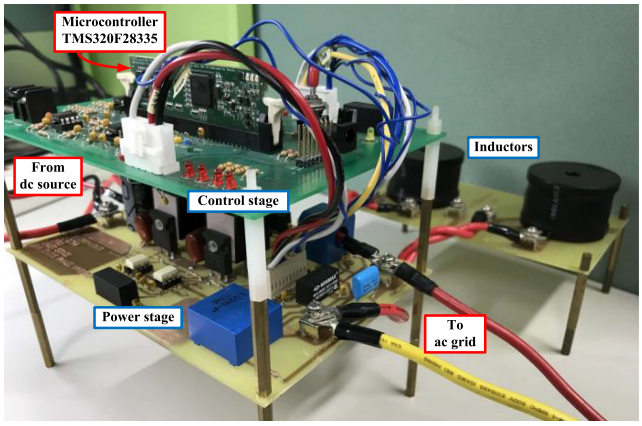

FIGURE 6. The picture of 1kVA prototype GVSI showing power stage and control stage with controller using TMS320F28355.

V. SIMULATION AND EXPERIMENTAL RESULTS

Table 3 presents the classification of the profiles for the GVSI to be tested under different ac mains voltages. For the GVSI power rating, the active power, P and reactive power, Q are set as 600 W and 800 VAR, respectively. These profiles are set as Normal, Case I and Case II where the values of Δv_{ac} are 0%, +15%, and −15%, respectively. Therefore, the expectation from these profiles is to observe the consistency of the output active and reactive power under various ac mains with different Δv_{ac} while using the proposed simplified equation (25) to replace the conventional equation (9). In the next section, computer simulations and hardware experimental results will be presented to verify the performance of the proposed simplified algorithm.

The performance of the proposed simplified equation (25) is tested by MATLAB/Simulink simulation and experimental measurement using prototype 1 kVA GVSI connected to the grid simulator as shown in Fig. 6.

A. COMPUTER SIMULATIONS

The proposed simplified algorithm is carried out using MATLAB/Simulink for different operating cases stated in Table 3. The simulation results for output power, ac mains voltage, and output current for different operating cases are shown in Fig. 7(a), (b), (c) and (d), respectively. For the waveform shown in Fig. 7(a), the instantaneous power maintains the same amplitude level for different operation cases. However, it experiences an avoidable disturbance between two cases when a very large ac line voltage step change occurs. As shown in Fig. 7(b), the ac mains voltage has a 15% sag during Case I and 15% swell in Case II. To produce the constant power, the current during Case I will be increased, as shown in Fig. 7(c),

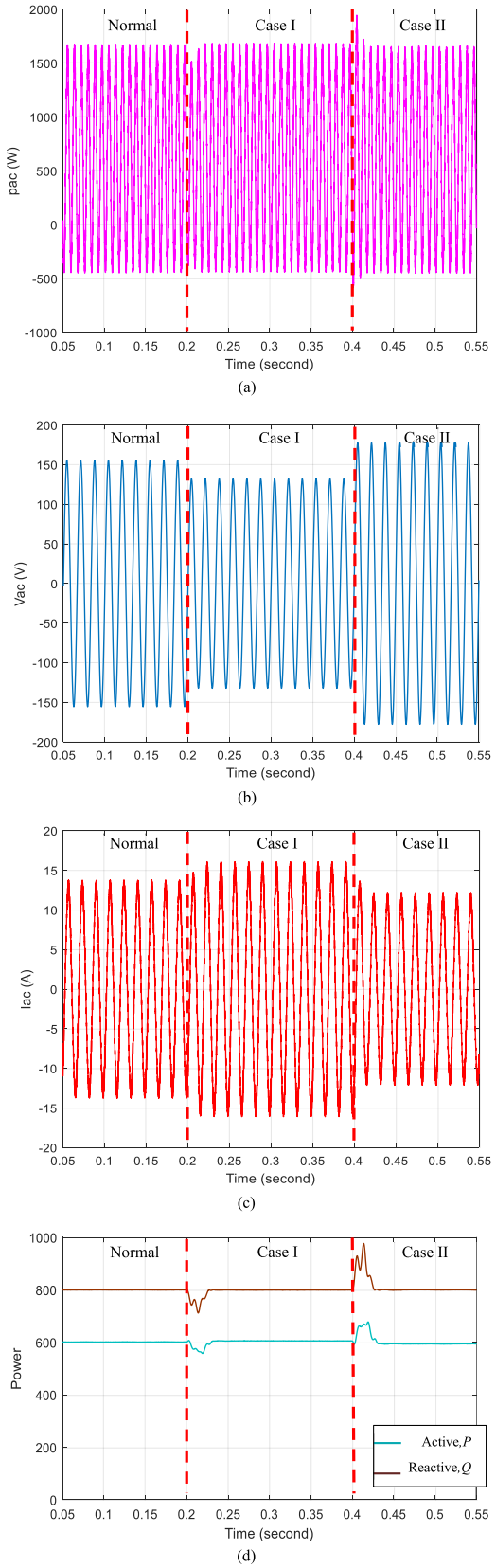

FIGURE 7. Simulation waveforms of (a) instantaneous power p_{ac}, (b) output voltage of the inverter v_{ac}, (c) output current of the inverter i_{ac} and (d) active and reactive power P and Q, respectively, under Normal, Case I, and Case II.

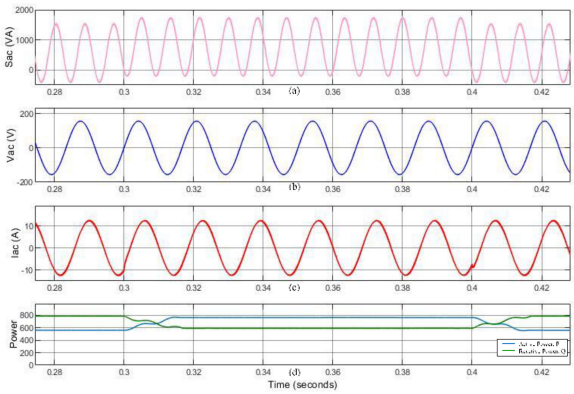

FIG. 8. Simulation waveforms of the inverter using the proposed simplified algorithm for the step change in demanded power under a constant grid voltage. From top to bottom: instantaneous power, p_{ac}; output voltage of the inverter, v_{ac}; output current of the inverter, i_{ac}; active power P and reactive power Q.

because of the change of the magnitude of the sinusoidal reference signal calculated by the proposed simplified (25). Similarly, the current in Case II will be reduced since the ac mains has a 15% voltage fluctuation. However, the output active and reactive power remain constant, as shown in Fig. 7(d), under different operation conditions. It should be mentioned that the proposed simplified algorithm can also achieve a fast transient response.

From the simulation results, it can be seen that the GVSI with the proposed simplified equation is able to maintain the demanded apparent power as the P and Q remain unchanged, even in different Case I and Case II.

It should be noted that the proposed simplified algorithm can achieve a fast transient response as shown in Fig. 7, where the current took one cycle to stabilize after a change in the ac mains voltage. From the simulation results, it can be concluded that the GVSI with the proposed simplified equation is able to maintain the demanded power under fluctuated ac mains voltages.

On the other hand, the proposed method also works well for any step change in demanded power under a constant grid voltage as the simulation results shown in Fig. 8. Besides, the proposed simplified algorithm can also achieve the desired performance under various frequencies and harmonics distortion. Because of the phase-lock-loop in the controller, both the conventional and the proposed simplified algorithm can generate the synchronized reference signal, which is in-phase with the line frequency, either 60 Hz or 50 Hz.

About the impact of the ac mains voltage harmonics, it is understandable that the performance of the injected P and Q will be affected by the ac mains voltage harmonics distortion. Fig. 9 shows the simulation results when the ac mains voltage is highly distorted with 20% THD consisting 3rd and 5th harmonics. It is reasonable that the output line current also contains harmonics components because of the distorted ac mains voltage. However, it can be seen that the inverter using the proposed simplified control method, as shown in

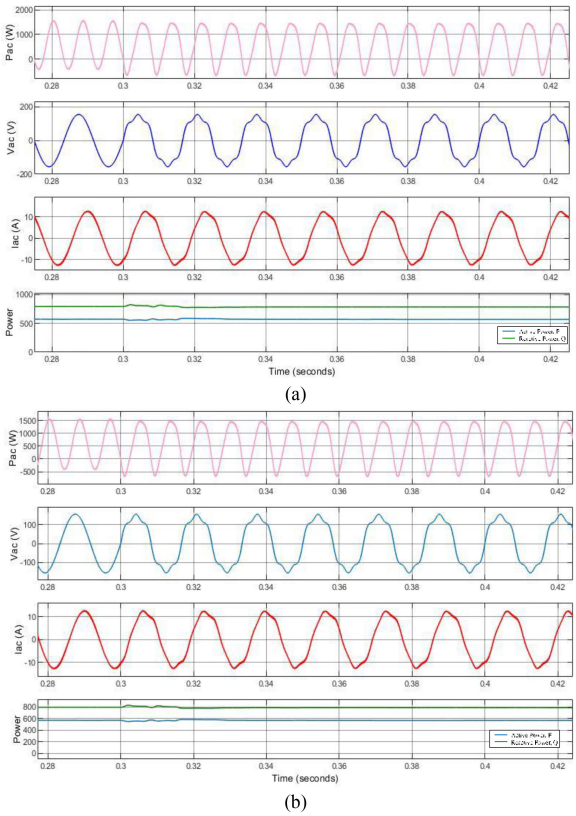

FIG. 9. Simulation waveforms of the inverter connecting to the distorted grid voltage with 20% THD at 0.3 sec. (a) using the conventional algorithm (b) using the simplified algorithm.

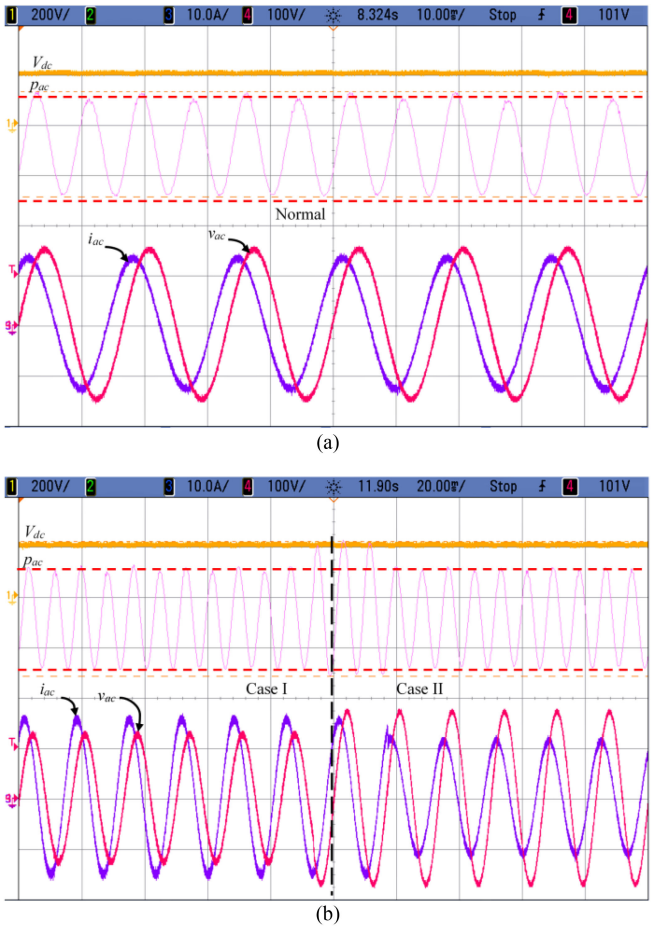

FIG. 10. Experimental waveforms of output voltage and current of the prototype GVSI, v_{ac} and i_{ac}, respectively (a) under Normal profile and (b) under Case I and Case II.

Fig. 9(b), can achieve almost the same performance by using the conventional control method, as shown in Fig. 9(a).

B. EXPERIMENTAL RESULTS

The picture of the prototype GVSI is shown in Fig. 6, where the control stage is stacked on the top of the power stage. The Texas Instruments DSP TMS320F28335 is adopted to realize the controller of the GVSI prototype. The grid voltage and output ac current are sensed and fed back to the controller to compensate the output current distortion. It should be mentioned that the demanded output power command is set by the user and the dc input voltage remains constant during the hardware experimental test.

The hardware experiments are conducted with the specifications shown in Table 1. The experimental setup consists of a Chroma programmable DC power supply 62100H-600S to supply constant dc voltage to the inverter and a Chroma programmable AC source 61611 as a grid simulator.

Fig. 10(a) shows the measured waveforms of the dc voltage V_{dc}, the instantaneous power p_{ac}, output voltage and current under the Normal profile listed in Table 3. It reveals that the prototype GVSI is able to inject an almost pure sinusoidal current into the grid to deliver the demanded active and reactive power. It should be noted that the small instantaneous power fluctuation is caused by the MATH function of the oscilloscope.

To validate the proposed algorithm, the prototype GVSI is tested with the classification profiles stated in Table 3. Fig. 10(b) shows the experimental results of the prototype GVSI operated under two different profiles of the Δv_{ac}.

In Fig. 10(b), from top to bottom, the yellow straight line is the dc voltage V_{dc}, the pink waveform is the instantaneous power p_{ac} obtained directly using the multiplication function of the oscilloscope, the purple one is the ac mains voltage v_{ac}, and the red one is the ac output current i_{ac} of the GVSI. As shown in Fig. 10(b), the ac mains voltage v_{ac} has different magnitudes in different cases. By using the proposed simplified algorithm, the ac line current will be adjusted accordingly. However, the envelope of the generated power p_{ac} remains unchanged during different ac mains profiles. The experimental results validate that the proposed simplified algorithm can successfully control the output current of the GVSI to deliver the consistent demanded power to the ac microgrid under a wide range of voltage variation.

It is worth to note that the proposed method also works well for any step change in demanded power under a constant grid voltage. In addition, the proposed simplified algorithm can also achieve the desired performance under various

frequencies and harmonics distortion. On the other hand, the reduction in computational burden through the proposed simplified algorithm offers the benefit to increase the switching frequency. Therefore, the size of passive components, such as the magnetic core, can be reduced too. Eventually, the reduction of size, weight, and cost of the converter becomes promising.

VI. CONCLUSION

The GVSI plays an important role for the energy storage component to connect to the microgrid. However, to deliver the demanded power to the grid, the reference signal of the controller needs to be calculated based on the variation of the ac mains voltage. In this paper, a simplified equation of the reference signal generation is proposed for the GVSI to reduce the computational burden while delivering the constant demanded power under various ac mains voltage. With the proposed simplified equations, the use of a low cost microcontroller unit becomes possible, the switching frequency can be increased, and the system's dynamic response can be improved. Also, the controller can save time resource to accomplish more tasks such as THD monitoring or multiple power module control. The operation principle of the GVSI current control using SPWM is introduced. The derivation of simplified equation under the variation of grid voltage is explained. The proposed simplified equation can reduce the computation burden by 52.3% with less than 0.62% of error. The performance of the proposed simplified algorithm is validated via mathematical calculations, computer simulations, and experimental results under various operation conditions.

REFERENCES

[1] A. M. Jadhav, N. R. Patne, and J. M. Guerrero, "A novel approach to neighborhood fair energy trading in a distribution network of multiple microgrid clusters," *IEEE Trans. Ind. Electron.*, vol. 66, no. 2, pp. 1520–1531, Feb. 2019.

[2] S. Dasgupta, S. K. Sahoo, S. K. Panda, and G. A. J. Amaratunga, "Single-phase inverter-control techniques for interfacing renewable energy sources with microgrid-Part II: Series-connected inverter topology to mitigate voltage-related problems along with active power flow control," *IEEE Trans. Power Electron.*, vol. 26, no. 3, pp. 732–746, Mar. 2011.

[3] S. Dasgupta, S. K. Sahoo, and S. K. Panda, "Single-phase inverter control techniques for interfacing renewable energy sources with microgrid-Part I: Parallel-connected inverter topology with active and reactive power flow control along with grid current shaping," *IEEE Trans. Power Electron.*, vol. 26, no. 3, pp. 717–731, Mar. 2011.

[4] A. M. Salamah, S. J. Finney, and B. W. Williams, "Single-phase voltage source inverter with a bidirectional buck-boost stage for harmonic injection and distributed generation," *IEEE Trans. Power Electron.*, vol. 24, no. 2, pp. 376–387, Feb. 2009.

[5] X. Hou *et al.*, "Distributed hierarchical control of AC microgrid operating in grid-connected, islanded and their transition modes," *IEEE Access*, vol. 6, pp. 77388–77401, 2018, doi: 10.1109/ACCESS.2018.2882678.

[6] Q. Li *et al.*, "Networked and distributed control method with optimal power dispatch for islanded microgrids," *IEEE Trans. Ind. Electron.*, vol. 64, no. 1, pp. 493–504, Jan. 2017.

[7] T. L. Vandoorn, B. Renders, L. Degroote, B. Meersman, and L. Vandevelde, "Active load control in islanded microgrids based on the grid voltage," *IEEE Trans. Smart Grid*, vol. 2, no. 1, pp. 127–139, Mar. 2011.

[8] S. M. Sharkh, M. A. Abusara, G. I. Orfanoudakis, and B. Hussain, "Introduction," in *Power Electronic Converters for Microgrids*, 1st ed., Singapore: John Wiley & Sons, 2014, pp. 1–12.

[9] M. Dabbaghjamanesh, A. Kavousi-Fard, and S. Mehraeen, "Effective scheduling of reconfigurable microgrids with dynamic thermal line rating," *IEEE Trans. Ind. Electron.*, vol. 66, no. 2, pp. 1552–1564, Feb. 2019.

[10] H. Zhang, W. Meng, J. Qi, X. Wang, and W. X. Zheng, "Distributed load sharing under false data injection attack in an inverter-based microgrid," *IEEE Trans. Ind. Electron.*, vol. 66, no. 2, pp. 1543–1551, Feb. 2019.

[11] H. Athari, M. Niroomand, and M. Ataei, "Review and classification of control systems in grid-tied inverters," *Renew. Sustain. Energy Rev.*, vol. 72, no. Oct. 2016, pp. 1167–1176, 2017, doi: 10.1016/j.rser.2016.10.030.

[12] N. Korada and M. K. Mishra, "Grid adaptive power management strategy for an integrated microgrid with hybrid energy storage," *IEEE Trans. Ind. Electron.*, vol. 64, no. 4, pp. 2884–2892, Apr. 2017.

[13] C. Vartanian, R. Bauer, L. Casey, C. Loutan, D. Narang, and V. Patel, "Ensuring system reliability: Distributed energy resources and bulk power system considerations," *IEEE Power Energy Mag.*, vol. 16, no. 6, pp. 52–63, 2018.

[14] K. Thirugnanam, S. K. Kerk, C. Yuen, N. Liu, and M. Zhang, "Energy management for renewable microgrid in reducing diesel generators usage with multiple types of battery," *IEEE Trans. Ind. Electron.*, vol. 65, no. 8, pp. 6772–6786, Nov.-Dec.2018.

[15] Z. Ma, A. Pesaran, V. Gevorgian, D. Gwinner, and W. Kramer, "Energy storage, renewable power generation, and the grid: NREL capabilities help to develop and test energy-storage technologies," *IEEE Electrif. Mag.*, vol. 3, no. 3, pp. 30–40, Sep. 2015.

[16] F. Katiraei, R. Iravani, N. Hatziargyriou, and A. Dimeas, "Microgrids management: Controls and operation aspects of microgrids," *IEEE Power and Energy Mag.*, vol. 6, no. 3, pp. 54–65, May/Jun. 2008.

[17] N. Pogaku, M. Prodanović, and T. C. Green, "Modeling, analysis and testing of autonomous operation of an inverter-based microgrid," *IEEE Trans. Power Electron.*, vol. 22, no. 2, pp. 613–625, Mar. 2007.

[18] J. Rocabert, A. Luna, F. Blaabjerg, and I. Paper, "Control of power converters in AC microgrids," *IEEE Trans. Power Electron.*, vol. 27, no. 11, pp. 4734–4749, Nov. 2012.

[19] T. C. Green and M. Prodanovi, "Control of inverter-based micro-grids," *Electr. Power Syst. Res.*, vol. 77, no. 9, pp. 1204–1213, 2007, doi: 10.1016/j.epsr.2006.08.017.

[20] Y. Wang, W. Xie, X. Wang, and D. Gerling, "A precise voltage distortion compensation strategy for voltage source inverters," *IEEE Trans. Ind. Electron.*, vol. 65, no. 1, pp. 59–66, Jan. 2018.

[21] T. B. Lazzarin, G. A. T. Bauer, and I. Barbi, "A control strategy for parallel operation of single-phase voltage source inverters: Analysis, design and experimental results," *IEEE Trans. Ind. Electron.*, vol. 60, no. 6, pp. 2194–2204, Jun. 2013.

[22] P. K. Sahu, R. K. Mahakhuda, S. Maity, and S. K. Samal, "A fixed switching frequency sliding mode control for single-phase voltage source inverter," in *Proc. 2014 Int. Conf. Circuits, Power Comput. Technol.*, 2014, pp. 1006–1010.

[23] H. Li, Y. Liu, J. Lu, T. Zheng, and X. Yu, "Suppressing EMI in power converters via chaotic SPWM control based on spectrum analysis approach," *IEEE Trans. Ind. Electron.*, vol. 61, no. 11, pp. 6128–6137, Nov. 2014.

[24] J. Lamb, B. Mirafzal, and F. Blaabjerg, "PWM common mode reference generation for maximizing the linear modulation region of CHB converters in islanded microgrids," *IEEE Trans. Ind. Electron.*, vol. 65, no. 7, pp. 5250–5259, Jul. 2018.

[25] L. Qin, M. Hu, D. D. C. Lu, Z. Feng, Y. Wang, and J. Kan, "Buck-boost dual-leg-integrated step-up inverter with low THD and single variable control for single-phase high-frequency AC microgrids," *IEEE Trans. Power Electron.*, vol. 33, no. 7, pp. 6278–6291, Jul. 2018.

[26] H. F. Xiao, K. Lan, and L. Zhang, "A quasi-unipolar SPWM full-bridge with constant common-mode voltage," *IEEE Trans. Power Electron.*, vol. 30, no. 6, pp. 3122–3132, Jun. 2015.

[27] M. Tofigh Azary, M. Sabahi, E. Babaei, and F. Abbasi Aghdam Meinagh, "Modified single-phase single-stage grid-tied flying inductor inverter with MPPT and suppressed leakage current," *IEEE Trans. Ind. Electron.*, vol. 65, no. 1, pp. 221–231, Jan. 2018.

[28] L. Hadjidemetriou, E. Kyriakides, Y. Yang, and F. Blaabjerg, "A synchronization method for single-phase grid-tied inverters," *IEEE Trans. Power Electron.*, vol. 31, no. 3, pp. 2139–2149, Mar. 2016.
[29] X. Liang and C. Andalib-Bin-Karim, "Harmonics and mitigation techniques through advanced control in grid-connected renewable energy sources: A review," *IEEE Trans. Ind. Appl.*, vol. 54, no. 4, pp. 3100–3111, Jul./Aug. 2018, doi: 10.1109/TIA.2018.2823680.
[30] C. H. Chang, F. Y. Wu, and Y. M. Chen, "Modularized bidirectional grid-connected inverter with constant-frequency asynchronous sigma-delta modulation," *IEEE Trans. Ind. Electron.*, vol. 59, no. 11, pp. 4088–4100, Nov. 2012.
[31] I. Texas Instruments, "C28x IQmath Library," *Module User's Guide SPRC990*, vol. V1.5c, pp. 1–80, 2010.

NOOR SYAFAWATI AHMAD (Member, IEEE) received the B.Eng degree in electrical engineering from Universiti Tun Hussein Onn Malaysia, Johor, Malaysia in 2008, and the M.Sc degree in electrical systems engineering from Universiti Malaysia Perlis, Perlis, Malaysia, in 2010. She is currently working toward the Ph.D. degree with Department of Electrical Engineering, National Taiwan University, Taipei, Taiwan. Her research interests include power electronic converters and renewable energy.

TERNG-WEI TSAI (Student Member, IEEE) received the B.S. degree in electrical engineering, in 2014, from National Taiwan University, Taipei, Taiwan, where he is currently working toward the Ph.D. degree. He has finished some projects with the Institute of Nuclear Energy Research, Atomic Energy Council, Taoyuan, Taiwan. He was a Teaching Assistant of Power Electronics Laboratory from 2018 to 2019. His research interests include three-phase grid-tied inverters, back-to-back active power conditioners, STATCOMs, and renewable energy systems.

YAOW-MING CHEN (Senior Member, IEEE) received the B.S. degree in electrical engineering from National Cheng Kung University, Tainan, Taiwan, in 1989 and the M.S. and Ph.D. degrees in electrical engineering from the University of Missouri, Columbia, MO, USA, in 1993 and 1997, respectively. From 1997 to 2000, he was with I-Shou University, Taiwan, as an Assistant Professor. From 2000 to 2008, he was with National Chung Cheng University, Taiwan. In 2008, he joined the National Taiwan University, Taipei, Taiwan, where he is currently a Professor in the Department of Electrical Engineering. His research interests include power electronic converters and renewable energy.